PAPER

Check for updates

Study of odd–even effects in physisorption and chemisorption of Ar, N₂, O₂ and NO on open shell Ag_{11-13}^{+} clusters by means of self-consistent van der Waals density functional calculations

Eva M. Fernández [ID] *[a] and Luis C. Balbás [ID] [b]

We have studied the adsorption and coadsorption properties of one or more X = Ar, N₂, O₂, and NO adsorbates on cationic silver clusters Ag_{11-13}^{+}, whose sizes are in the open shell region of metal clusters, aiming to understand the observed odd–even effects in the abundance spectra of $Ag_{11-13}^{+} \cdot m$X complexes. All calculations were performed self-consistently using a non-local van der Waals correlation functional, covering the different nature of the interactions between the silver substrate and the several adsorbates, which range from dispersion (London) forces for Ar, non covalent π–π interactions for N₂, charge-transfer interactions for O₂ and NO, and the covalent Ag–Ag bond in the nude silver cluster. Despite the wide interval of adsorption energies, spanning two orders of magnitude, we have been able to explain the following experimental facts. For X = Ar, N₂, and O₂ reactions with Ag_{11-13}^{+}, it was observed in the mass spectra an abundance peak at n = 12 [M. Schmidt, et al., ChemPhysChem, 2015, **16**, 855]. In addition it was observed the competitive adsorption of two or more N₂ molecules, and the cooperative effect of adsorbing N₂ together with O₂ molecules. For X = NO, an abundance peak at n = 12 has been also observed [J. Ma, et al., Phys. Chem. Chem. Phys., 2016, **18**, 12819]. We find that the main factors determining these properties are the different core motifs of the cluster geometry (pentagonal bipyramid for Ag_{11}^{+} and Ag_{13}^{+}, but triangular prism for Ag_{12}^{+}) and, on the other hand, the odd number of valence electrons for Ag_{12}^{+}, leading to a smaller HOMO–LUMO gap than those of its neighbours. Further details about the preferred adsorption sites, dipole moments, and dipole polarizabilities are also discussed.

1 Introduction

Aside from their application in many branches of nanotechnology based products such as, for example, antimicrobial agents,[1] silver nanoparticles are being studied currently as a support for small molecules and radicals (N₂, O₂, NO, etc....), focussing on the understanding of their catalytic properties.[2,3] Much of the recent effort in this direction has dealt with neutral and anionic nanoparticles,[4–11] but interesting results have been also found recently for positively charged clusters.[2,11–14] The reactivity of bimetallic $Ag_nM_m^{0\pm}$ clusters towards small particles has been also explored.[15–18] The interaction of pure and bimetallic clusters with noble gases, like argon, has been studied in order to infer the particle morphology and to characterize its physisorption activity.[2,19]

Bréchignac and coworkers[2,12] have extracted and rationalized general size-dependent trends about the reactivity of cationic silver clusters by analyzing the mass spectra of gas phase Ag_n^{+}X clusters (n ≤ 70), X being one or more of Ar, N₂, and O₂ adsorbed molecules. For noble gases, the interaction was unambiguosly characterized as physisorption. However, the connection between the observed stability pattern of $Ag_n^{+} \cdot m$Ar complexes and the cluster geometry could not be clearly established. With respect to N₂, they found that the adsorption signal behaves as that of rare gases, that is, in both cases the adsorption decreases with cluster size and shows peaks at the same sizes, suggesting that N₂, like noble gases, suffers physisorption. On the contrary, for oxygen adsorption, the mass spectra data indicate that molecular oxygen is chemisorbed (at 77 K) on Ag_n^{+} up to at least n = 70, and the signal increases with cluster size. As a unified explanation of these general trends, Bréchignac and coworkers[2,12] conclude that the factor responsible for both N₂ physisorption and O₂ chemisorption is the surface charge density on the cluster cations, since it promotes N₂ physisorption and hinders electron transfer to O₂, and both effects decrease when the surface charge density

[a] Departamento de Física Fundamental, Universidad Nacional de Educación a Distancia, Madrid, Spain. E-mail: emfernandez@fisfun.uned.es
[b] Departamento de Física Teórica, Universidad de Valladolid, 47011 Valladolid, Spain

decreases as the cluster size increases. Superposed onto these general adsorption trends, notorious variations with cluster size are observed, which are attributed to very different causes depending on the type of adsorbate and the electronic and geometric structure of the particular Ag_n^+ cluster. Thus, calculations for small size Ag_n^+ clusters[12] show that the binding energy of N_2 positively correlates with the coordination number of adsorption sites, and that physisorption at obtuse corners is stronger than that at acute ones. It was also observed competition between multiple N_2 physisorptions on small clusters,[2,12] that is, physisorption of N_2 at any site is reduced by the presence of other N_2 molecules on other sites. Another experimental fact is that those clusters with an adsorbed O_2 molecule are able to attract more nitrogen than bare clusters. This cooperative effect is consistent with charge transfer from the cluster to the O_2 molecule, which enhances the positive charge on the metallic part of the cluster, thus promoting N_2 physisorption.

DFT calculations for neutral Ag_n clusters ($n \leq 9$) have predicted that dissociation of O_2 is preferred for larger sizes, while molecular adsorption is favored for $n \leq 5$ sizes.[7] Dissociation of O_2 is reported in experiments[12,15] at temperatures higher than about 100 K. (Our calculations in the present paper are conducted at 0 K.) On the other hand, electronic shell closing effects, and the electron pairing energy,[9] arising from a small number of confined interacting electrons, originate the peaks and valleys which appear superimposed on the increasing trend with the size of cationic silver clusters with chemisorbed O_2 molecules.[2] In the range of sizes $n = 11$–13, where no electronic shell closing effects occur, it can be expected subshell splitting due to oblate distortion of the geometry,[13,20] in addition to the odd–even effect caused by the electron pairing energy. Oxygen, as an electron acceptor, reacts with alkali and alkaline-earth species. Thus, it is observed that the alkaline-earth-like Ag_{11}^+ (ten valence electrons) chemisorbs O_2 despite its paired electron configuration. Instead, even-n cationic clusters, which have an unpaired electron, are unreactive when they are just below the noble gas configurations, such as Ag_8^+ and Ag_{19-20}^+. However, clusters with an unpaired electron not far above the noble gas configuration, such as Ag_{12}^+, behave like an alkaki superatom and transfer that electron to O_2, which will appear as a superoxo-like chemisorbed molecular oxygen. No more than a single O_2 molecule adsorbed on Ag_n^+ with $n < 22$ was observed.[2]

As noticed by Khanna and coworkers[8] for Ag_{13}^-, anionic clusters with an odd number of Ag atoms (an even number of electrons) require spin accommodation to activate the O–O bond since the antibonding orbitals of the O_2 (triplet ground state) are filled. That spin conservation rule should hold also for cationic clusters. Thus, triplet oxygen reacts rapidly with all species in a doublet spin state (and possibly higher spin states), whereas it reacts much more slowly with species in a singlet state,[21] that is, clusters with low spin excitation energy bind O_2 strongly and then are more reactive. High spin excitation energy results from a distortion in the geometry, leading to a splitting of the D shell, and then to a large electron detachment energy and HOMO–LUMO gap at the subshell level.

As proposed by Khanna and coworkers,[8] the ability of clusters to accommodate spin excitation and the modification of electronic shells *via* geometrical distortions can explain the observed variable reactivity of silver clusters with oxygen. That reasoning was also used to explain the observed odd–even effects in the reactivity of Al_n^- and Ga_n^- ($n = 9$–14) towards molecular oxygen.[22] Similar ideas concerning the role of the structural isomers in the adsorption of NO on Cu_{13} have been also argued in a recent theoretical study by Iwasa and coworkers.[23]

Small silver clusters are supposed to be the active phase in the Ag/Al_2O_3 catalyst for selective catalytic reduction of nitrous oxides, NO_x, in the presence of hydrocarbons[24,25] and ammonia.[26] As a first step to understand these processes, apart from the action of the support, density functional calculations have been done to explore NO_x adsorption on pure and doped silver clusters,[7,18] as well as the Ag(111) surface[27] and AlN(0001) surface.[28] DFT calculations show that NO interacts weakly with Ag_n clusters ($n \leq 8$) and is preferably adsorbed in atop sites.[7] Experiments of adsorption and activation of NO on silver clusters with sizes up to one nanometer show that the interactions are dominated by electron transfer from silver to NO.[11] The adsorption of NO on Ag_nRh ($n \leq 15$) occurs with enhanced reactivity compared to that on pure Ag_n.[18] Calculations of NO adsorption on the Ag(111) surface[27] predict that all high symmetry sites on the Ag(111) surface are stable, with binding energy ranging from 0.17 (top) to 0.33 (fcc site). At fcc and bridge sites the NO axis is nearly perpendicular to the surface, while at the top site the NO axis is about $33°$ off the surface normal.

In this work we study, by means of spin dependent DFT calculations, the odd–even electronic effects on the the reactivity of Ag_{11-13}^+ clusters towards one or more Ar, N_2, and O_2 molecules, as well as the conjoint adsorption of N_2 and O_2. In addition we will consider the non dissociative adsorption of NO as a first step in the search for dissociation pathways of NO from several low-lying energy Ag_{11-13}^+ structural isomers. In Section 2 we give details of the computational method used in this work. Section 3 contains the results and discussion organized in subsections for (i) pure cationic silver clusters, (ii) adsorption of one to three Ar atoms on these clusters, (iii) adsorption of one and two N_2 molecules, (iv) adsorption of a single O_2 molecule, (v) co-adsorption of O_2 and N_2 molecules, and (vi) adsorption of a single NO molecule. Conclusions are given in Section 4.

2 Computational methods

In this work, DFT calculations were performed using the code SIESTA[29] with the self-consistent exchange and correlation potential given by the non local van der Waals (vdW) density functional of Klimes, Bowler, and Michaelides (KBM).[30] The core interactions were accounted for by means of norm conserving scalar relativistic pseudopotentials[31] in their fully non-local form,[32] generated from the atomic valence configuration $4d^{10}6s^16p^0$ for Ag, $2s^22p^4$ for O, $2s^22p^3$ for N and $4s^24p^6$ for Ar. The core radii for (s, p, d) orbitals are, in a.u., (2.49, 2.59, 2.20),

(1.13, 1.13, 1.13), (1.23, 1.23, 1.23) and (1.58, 1.58, 1.84) for Ag, O, N and Ar, respectively. The pseudopotentials of Ag, O and Ar have been tested in previous work.[6,33] For the N_2 dimer we obtain a binding energy 4.72 eV, and a bond length 1.13 Å, to be compared to the measured values 4.90 eV and 1.10 Å, respectively. For $^3O_2$ the calculated (experimental) values of the binding energy and bond length are 3.227 eV (2.558 eV) and 1.247 Å (1.208 Å), respectively. For the NO molecule, these values are 7.050 eV (6.515 eV) and 1.185 Å (1.151 Å), respectively.

The matrix elements of the self-consistent potential were evaluated by integrating using a uniform grid. The grid fineness is controlled by the energy cutoff of the plane waves that can be represented in it without aliasing (150 Ry in this work). Flexible lineal combinations of numerical pseudo-atomic orbitals (PAO) are used as the basis set, allowing for multiple-ζ and polarization orbitals. Here we use DZ plus a p polarization orbital. To limit the range of PAOs, they were slightly excited by a common energy shift (0.001 Ry in this work) and truncated at the resulting radial node, leading to maximum cutoff radii, in au, of 9.49 (s), 5.73 (p), 6.39 (p) and 6.11 (p) for Ag, O, N and Ar, respectively. In the self-consistent field calculations, the density and energy tolerances were set to 10^{-4} e Bohr^{-3} and 10^{-3} eV, respectively. The equilibrium geometries resulted from unconstrained conjugate-gradient structural relaxation using the DFT forces until the force on each atom was smaller than 0.001 eV Å^{-1}. We considered several initial structures for each cluster taken from the low lying energy isomers of neutral and charged Ag clusters obtained in previous work using a number of different DFT approaches.[8,9,14,34–38] Our calculations in the present paper are conducted at 0 K.

We use the KBM self-consistent non local van der Waals density functional[30] to properly take into account the electronic dispersion effects that occur in the physisorption of Ar and N_2 on silver clusters. This kind of functional is essential to accurately describe critical electronic properties of metallic systems, such as the dipole moment and static polarizability of sodium[39] and gold[33] clusters. Another example is the explanation of the photoelectron spectrum of Au_{12}^-, for which detailed experimental features[40] are well described theoretically by a suitable combination of the density of states of a planar isomer and that of a three-dimensional isomer,[33] both obtained with the KBM exchange–correlation functional. Recent benchmarking of several van der Waals dispersion approaches[41] shows that the vdW-DF2 kind of functionals (KBM used here is one of them) perform better than those semiempirical functionals based on many body dispersion methods, when compared with CCSD(T) results for the intermolecular interaction energy in a large set of test molecules. We have performed GGA/PBE calculations for pure cationic silver clusters and for the adsorption of a single molecule of Ar, N_2, and O_2. The sequence of isomers of pure clusters in Table 1 only changes for the first and second isomers of Ag_{11}^+. The adsorption energy of Ar (N_2) is larger (smaller) using VDW than using GGA/PBE, and the adsorption energy of O_2 is nearly the same within both functionals. The higher computational costs of the vdW-DF2 self consistent treatment compared to those of semiempirical and single point treatments are compensated by the improved theoretical description, which is reflected in better understanding of the studied physisorption and chemisorption processes.

3 Results and discussion

3.1 Structure of Ag_n^+ clusters with n = 11–13

In Fig. 1 are presented the optimized equilibrium geometries of three low energy Ag_n^+ clusters with n = 11 (first row), n = 12 (second row), and n = 13 (third row). The two numbers below each geometry are the total energy (in eV) with respect to the lowest energy isomer, and the modulus of the electrical dipole moment. The orientation of the dipole moment for each structure is indicated by an arrow.

We observe that the lowest energy geometries of Ag_{11}^+ and Ag_{13}^+ are both grown from a pentagonal bipyramid (whose axis is along the line joining two atoms labeled with a black star in Fig. 1). For the lowest energy Ag_{11}^+ isomer we see an additional pentagonal bipyramid whose axis is an edge of the other pentagon (and *vice versa*). The nearly degenerate isomer of Ag_{11}^+ at only 0.004 eV higher energy, which will be denoted as Ag_{11}^+* in the following, contains also a pentagonal bipyramid motif, with three Ag atoms capping three consecutive faces on a side of the pentagon plane, and another Ag atom bridging one edge of the pentagon and bonding to one of the capping atoms. The geometrical motif of the third isomer of Ag_{11}^+ in Fig. 1 is a triangular prism, whose edge connecting the acute corners of the triangles is marked with red cross symbols. The lowest energy geometry of Ag_{12}^+ contains a triangular prism motif, with five Ag atoms capping their five faces (three squares and two triangles) plus another Ag atom binding to the Ag caps of a triangle and a square. The second isomer of Ag_{12}^+ is formed by a compact arrangement of tetrahedra, and the third isomer shows the pentagonal bipyramid motif. The lowest energy isomer of Ag_{13}^+ contains again the pentagonal bipyramid motif, and the second

Table 1 In the columns from left to right are given, for $Ag_{11–13}^+$ clusters in their minimum energy state, the cluster symbol, spin multiplicity, binding energy per atom (see eqn (1)), mean Ag–Ag bond length, HOMO–LUMO gap, average coordination (twice the average number of bonds per atom; the maximum Ag–Ag distance is fixed to 2.9 Å), modulus of the dipole moment (see eqn (2)), mean static dipole polarizability (see eqn (4)), and polarizability anisotropy (see eqn (5)). The isomer Ag_{11}^+*, at only 0.004 eV higher total energy than Ag_{11}^+ (see Fig. 1), is also included

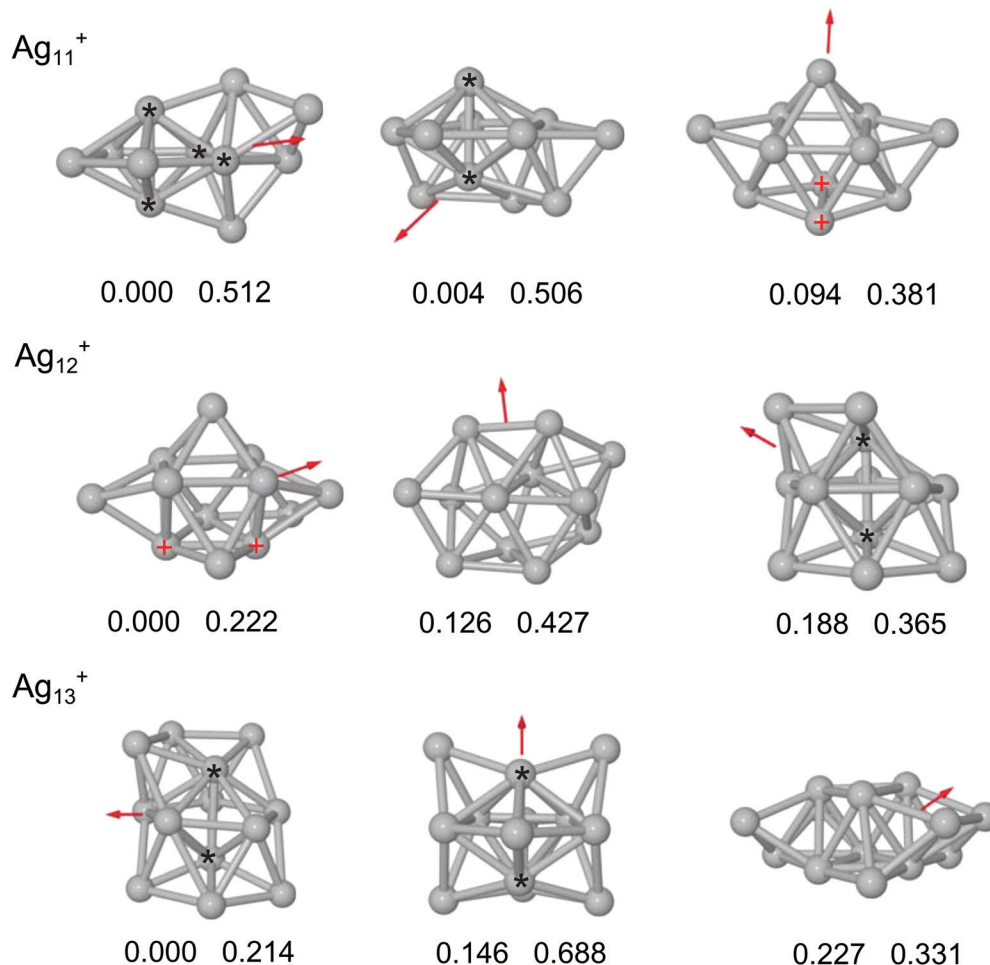| Cluster	$2S + 1$	E_{bind} (eV)	$\bar{d}_{Ag–Ag}$ (Å)	H–L (eV)	$\langle Coor.\rangle$	$|\mu|$ (Debye)	$\bar{\alpha}/n$ (Å^3)	$\Delta\alpha/n$ (Å^3)
Ag_{11}^+	1	1.745	2.838	1.121	3.454	0.512	5.476	2.682
Ag_{11}^+*	1	1.745	2.839	0.732	3.272	0.507	5.278	2.140
Ag_{12}^+	2	1.734	2.856	0.117	4.000	0.227	5.283	1.870
Ag_{13}^+	1	1.772	2.806	0.770	2.924	0.214	5.358	3.099

Fig. 1 In the first, second, and third rows are shown the geometries of three low energy isomers of Ag_{11}^+, Ag_{12}^+, and Ag_{13}^+, respectively. Below each geometry is given the energy (in eV) with respect to the lowest energy isomer, and the modulus of the electric dipole moment (in Debye). The arrow attached to the structures indicates the direction of the dipole moment. Other electronic and structural properties are given in Table 1. In this figure we emphasize that most geometries contain either a pentagonal bipyramid motif (whose axis is denoted by two black star (*) symbols), or a triangular prism motif (with the side conecting the two acute corners marked with two red cross symbols).

isomer maintains that motif. This second isomer was also found by Chen and coworkers[9] as the third isomer of the neutral species. The third isomer of Ag_{13}^+ in Fig. 1 is a bilayer structure which was also found by Khanna and coworkers[13] as the first isomer of the cationic species.

Certainly, we do not pretend to establish a general law for the structural motifs of cationic silver clusters in the range of sizes 7–13 atoms. Simply, by checking previous work (*e.g.* ref. 37 and references therein), we have verified that the geometry of many low lying energy isomers in that range contains either the triangular prism or the pentagonal bipyramid as a structural motif. Then, we realize that the lowest energy isomer of Ag_7^+, Ag_9^+, Ag_{11}^+ and Ag_{13}^+ contains the pentagonal bipyramid, whereas the triangular prism motif appears in the lowest energy isomer of Ag_{10}^+ and Ag_{12}^+ (but not in Ag_8^+).

The relation between the electronic and ionic structure of metal clusters with nearly free valence electrons, such as the alkali and the noble metal ones, is far from being understood, apart from some semi-phenomenological rules provided by the non-spherical jellium model for those cases with non closed

electronic shells.[42] Here we study the odd–even structural effect in $Ag_{11–13}^+$ clusters, that is, the alternation of pentagonal bipyramid and triangular prism motifs, on the adsorption properties of Ar, N_2, and O_2 on these non-closed shell clusters.

The interplay between the atomic geometry and odd–even electron number with respect to the reactivity of neutral and negatively charged silver clusters towards O_2, in the region of sizes n = 8–18 atoms, has been examined by Khanna and coworkers.[8,13,43] The clusters in that region, whose shell model electronic configuration evolves from $1S^2 1P^6$ to $1S^2 1P^6 1D^{10}$ closed shells, suffer subshell splitting and strong rearrangement of the $1P_x$, $1P_y$, $1P_z$, $1D_{z^2}$, $1D_{xz}$, $1D_{yz}$, $1D_{xy}$, and $1D_{x^2-y^2}$ subshells due to a deviation from the nearly spherical atomic geometry.[20,42] Thus, for silver clusters with 10–14 valence electrons, the atomic arrangement is prolate (the cluster geometry spreads along one axis more than along the other two axes). Nevertheless, the detailed arrangement of the different S, P, and D subshells depends on the charge state. For example, calculations for 14 valence electron silver clusters (Ag_{15}^+, Ag_{14}, and Ag_{13}^-) show that the HOMO level has different orbital character (subshell),

which is more important for the reactivity, and also a different HOMO–LUMO gap.[8,13,43] Apart from the HOMO–LUMO gap, other possible manifestations of the splitting and rearrangement of subshells (which can also be understood as a crystal field splitting of the jellium-model energy levels) are the inexistence of odd–even effects in the calculated removal energy of one[13] and two[14] Ag atoms out of Ag_{10-14}^+ clusters, as well as in their average binding energy.[9,14]

In Table 1 are given the spin multiplicity, binding energy per atom, average bond length, HOMO–LUMO gap, and the average coordination per atom for the smallest energy configuration of Ag_{11-13}^+ clusters and for the nearly degenerate isomer Ag_{11}^{+*}, which has only 0.004 eV higher total energy than Ag_{11}^+. In the last three columns of Table 1 are given the modulus of the dipole moment, the mean dipole polarizability, and the the polarizability anisotropy. The binding energy per atom is defined in eqn (1), where $E(X)$ is the total energy of species X:

$$E_{bind}(Ag_n^+) = [(n-1)E(Ag) + E(Ag^+) - E(Ag_n^+)]/n \qquad (1)$$

We see in Table 1 that the binding energy is higher for odd n than for even n clusters, that is, those clusters with an even number of electrons have extra binding energy, which can be attributed to the electron pairing energy.[9] Thus, having a higher multiplicity has a cost in the binding energy of silver clusters with few 1D valence electrons. This fact is also noticeable in the HOMO–LUMO gap. It is well known that clusters with higher HOMO–LUMO gaps are less reactive than those with smaller ones. With respect to structural effects, the average bond length and the average coordination number are both larger for Ag_{12}^+ (odd number of electrons) than for Ag_{11}^+ and Ag_{13}^+. We will see below that these properties are related to the physisorption interaction with Ar and N_2 molecules. The smaller binding energy of Ag_{12}^+ with respect to its neighbours correlates with its smaller abundance observed in mass spectra, see, for example, the recent results by Luo and coworkers.[44] (Incidentaly, the geometry reported by Luo and coworkers[44] as the ground state of Ag_{11}^+ corresponds to that of our isomer at 0.094 eV higher energy shown in Fig. 1.)

The electric dipole moment is obtained from the numerical integration

$$\mu_j = -e \int r_j \rho(\mathbf{r}) d^3 r + eZ \sum_{\mathbf{R}} R_j \qquad (2)$$

where r_j and R_j are electronic and nuclear Cartesian coordinates, respectively, $\rho(\mathbf{r})$ is the electron density, and Z is the ionic charge. The static dipole polarizability can be obtained from the induced component of the dipole moment in the presence of an external electric field $\mathbf{F}$:[39]

$$\alpha_{ij} = \frac{\mu_j(+F_i) - \mu_j(-F_i)}{2F_i}, \quad i,j = x,y,z. \qquad (3)$$

In the polarizability calculations, we employ external electric field values $F_i = 0.000$ and ± 0.002 a.u. along the three Cartesian directions, a total of six additional calculations for each cluster.

For each value of the external electric field, we self-consistently optimize both the electron density and the structure of the cluster with the same force tolerance (1 meV Å^{-1}) as in the zero field calculations. We assume that the chosen field intensities are well within the linear regime, where the above relations for the polarizability are valid. Test calculations for Ag_{11}^+ with $F_i = 0.000$ and ± 0.001 a.u. do not change the result significantly. The three diagonal elements of the polarizability tensor are extracted from the linear fits of the dipole moment components against the external field components, and the mean polarizability is calculated as

$$\bar{\alpha} = Tr(\alpha_{ij})/3. \qquad (4)$$

The polarizability anisotropy is calculated (ignoring the non diagonal α_{ij} elements) as

$$\Delta\alpha = \frac{1}{\sqrt{2}}[(\alpha_{xx} - \alpha_{yy})^2 + (\alpha_{yy} - \alpha_{zz})^2 + (\alpha_{zz} - \alpha_{xx})^2]^{\frac{1}{2}}. \qquad (5)$$

Notice in Table 1 that Ag_{12}^+ has the smaller polarizability with the smaller anisotropy value (except the low lying isomer Ag_{11}^{+*}, whose $\bar{\alpha}/n$ value is only 0.005 Å^3 smaller).

The modulus of the calculated dipole moments in Table 1 indicates that $n = 11$ cations are about twice more polar than $n = 12$ and $n = 13$ ones. In Fig. 1 is indicated by an arrow the direction of the dipole moment. The electric dipole moment is very sensitive to the precise nuclear positions, and different theoretical methods can predict different global minimum structure and also different electronic screening properties (and shape distortions), which affect the μ-value. The localization of holes of charge on the clusters, that is, the information about the dipole moment, is given in Fig. 1 in a crude gross manner. More specifically, Bader analysis shows that all the atoms in the cationic silver clusters lost charge with respect to their charge in the neutral cluster, and the minimum (maximum) charge lost by a single atom is -0.056, -0.041, and -0.037 (-0.121, -0.127, and -0.123), in $|e|$ units, for clusters with 11, 12, and 13 atoms, respectively. Interestingly, for the Ag_{11}^{+*} isomer the minimum and maximum loss of charge are -0.014 and -0.146, respectively.

The dipole contribution to the measured effective cluster polarizability at finite temperature T is[45]

$$\alpha_{eff} = \bar{\alpha} + \frac{\mu^2}{3kT}, \qquad (6)$$

where k is Boltzmann's constant. That correction is important at low temperatures for clusters with permanent dipole moments. Using the values of $\bar{\alpha}$ and μ of Table 1 in eqn (6) we estimate that the effective polarizability α_{eff} of Ag_{12}^+ should be equal to that of Ag_{13}^+ at ~ 185 K, a temperature higher than that in the experiments of Bréchignac and coworkers,[2] and far beyond the validity of eqn (6).

The calculated mean polarizabilities per atom of Ag_{11-13}^+ clusters given in Table 1 are slightly smaller than those calculated for isoatomic neutral species.[13,46] Since the mean static polarizability of metallic clusters is related directly to the volume of the (electron cloud of the) cluster,[42,47] the difference

between the polarizability of cationic and neutral species is due to the smaller size of the cation electron cloud with respect to that of its neutral species. On the other hand, the odd–even alternation of the mean polarizability per atom is related to the odd–even number of valence electrons, or, correspondingly, the even–odd number of atoms.[46] Khanna and coworkers[13] found that neutral silver clusters with odd-numbers of atoms have larger polarizability per atom than those with even-numbers of atoms by about 0.1 Å^3 per atom. That difference is smaller than that found here between the two isomers of Ag_{11}^+, see Table 1, which, then, should be due to their different geometry. Notice in Table 1 that the average Ag–Ag distance and the average coordination are not very different for the Ag_{11}^+ and Ag_{11}^{+*} isomers, indicating a similar size of the ionic structure. The dipole moments of these isomers have also similar values. However, the size of their electron clouds, as measured by the dipole polarizability, is clearly different. Also their HOMO–LUMO gap values substantially differ. Then, the subtle difference in the electronic configurations, particularly the electronic spill-out of the valence electron cloud induced by the different geometry of these isomers, is responsible for their different polarizability and HOMO–LUMO gap values. The electronic spill-out, δ, is defined as the difference between the radii of the electron cloud ($\bar{\alpha}^{1/3}$) and the jellium model ($r_{WS}n^{1/3}$), where r_{WS} is the Wigner–Seitz radius, whose experimental value[48] is 1.60 Å. Thus, for n = 11, 12, and 13, the spill-out values are (in Å) 0.362, 0.324, and 0.352, respectively (0.314 for Ag_{11}^{+*}).

With respect to neutral silver clusters, in the range of sizes n = 9–15 there are available polarizability measurements[49] only for clusters with odd numbers of atoms (n = 9, 11, 13, and 15). Calculations for neutral silver clusters by McKee and Samokhvalov[14] led to polarizability values slightly decreasing in the range n = 11–14. Older calculations[13,46] led to very small differences (<0.07 Å^3 per atom) between odd and even values of polarizability in that range of sizes, with valleys at even numbers of atoms (up to n = 13). Our calculations for the mean polarizability of cationic silver clusters with n = 11–13 (see Table 1) show an odd–even behaviour, with a valley at n = 12 (odd number of electrons). We stress again that calculated dipole moments, which we use to calculate the dipole polarizability tensor by means of eqn (3), are very sensitive to the cluster geometry and to the level of exchange–correlation description used in calculations.[33,39]

In this work we will use the mean polarizability as a quantitative indicator of the volume of the electron cloud, and the polarizability anisotropy as an index of the asphericity of that electron cloud. One consequence of the anisotropy, $\Delta\alpha$, is that the dispersion force between molecules becomes dependent on their mutual orientation, originating steric forces, which may be repulsive. Although Ag_{12}^+ has a larger Ag–Ag average distance than its neighbour clusters, its polarizability (the volume of its electron cloud) is smaller. As the volume is a physical property, related to the amount of space occupied by the particle, the polarizability and polarizability anisotropy of silver clusters will have some relevance in the physisorption interactions with different atoms and molecules that we study

in this work. On the other hand, we will use the HOMO–LUMO value as an indicator of stability against electronic transitions. Clusters with unpaired valence electrons are, in principle, more reactive to chemisorption interactions than those with paired electrons.

3.2 Physisorption of 1, 2, and 3 Ar atoms

For m = 1–3 and n = 11–13, we have probed all possible configurations of $Ag_n^+ \cdot Ar_m$ complexes resulting from adding an Ar atom to the lowest energy isomer $Ag_n^+ \cdot Ar_{m-1}$. Throughout this paper we will denote with a dot the physisorption of particle X on Ag_n^+ clusters: $Ag_n^+ \cdot X$.

In the first to fourth columns of Fig. 2 are shown the lowest energy geometries of silver–Ar complexes formed after adsorption of m = 1, 2, and 3 Ar atoms (first, second, and third row, respectively) on Ag_{11}^+ (first column), Ag_{11}^{+*} (second column), Ag_{12}^+ (third column), and Ag_{13}^+ (fourth column). In all cases the Ar atoms are adsorbed on top of Ag atoms whose coordination is smaller than the average one (except for $Ag_{13}^+ \cdot mAr$ and $Ag_{11}^+ \cdot 2Ar$, see Table 2) and the substrate geometry is not modified after absorption.

In Table 2 are given the adsorption energy (see eqn (7)), the bond distance Ar to the cluster, the site coordination ratio, and the charge accumulated on the Ar atoms, for one, two, and three Ar atoms adsorbed on Ag_{11-13}^+ clusters. The coordination ratio is defined as the quotient between the coordination of the adsorption site and the average coordination of the cluster given in Table 1. To obtain the coordination ratio the maximum Ag–Ag distance was fixed at 2.9 Å.

The adsorption energy of an atom/molecule X on the $Ag_n^+ \cdot mX$ complex is defined as:

$$E_{ads} = E(Ag_n^+ \cdot (m-1)X) + E(X) - E(Ag_n^+ \cdot mX) + \Delta ZPE \quad (7)$$

where $E(Y)$ is the total energy of species Y, and

$$\Delta ZPE = ZPE(Ag_n^+ \cdot (m-1)X) + ZPE(X) - ZPE(Ag_n^+ \cdot mX), \quad (8)$$

is the contribution of the zero point energy (ZPE) correction.

The accumulated charge on one, two, and three adsorbed Ar atoms given in Table 2 is calculated by means of the Bader method[50] (using a cutoff energy of 300 eV). Notice that the charge on the first adsorbed Ar atom will change after the adsorption of the second Ar atom, and so on. Thus, the Ar atom adsorbed on $Ag_{11}^+ \cdot 2Ar$ brings the accumulated charge on the Ar atoms from -0.022 $|e|$ to -0.015 $|e|$, that is, the third Ar atom acts as an electron acceptor instead of an electron donor.

As for the kind of interactions between rare gases and cationic silver clusters, it was suggested by experiments[2] that they were not chemical, but of physical character instead, leading then to physisorption rather than chemisorption processes. This suggestion is confirmed by inspecting in Table 2 the small adsorption energy (column 2), the large bond-length (column 3), and the small charge on Ar atoms (column 5) for one, two, and three Ar atoms adsorbed on Ag_{11-13}^+ clusters. In addition, we can observe odd–even effects in the trends of these magnitudes with size. Thus, for n = 12 complexes, the distance Ar–Ag is larger, and the binding energy is smaller, than for their n = 11 and n = 13 neighbours.
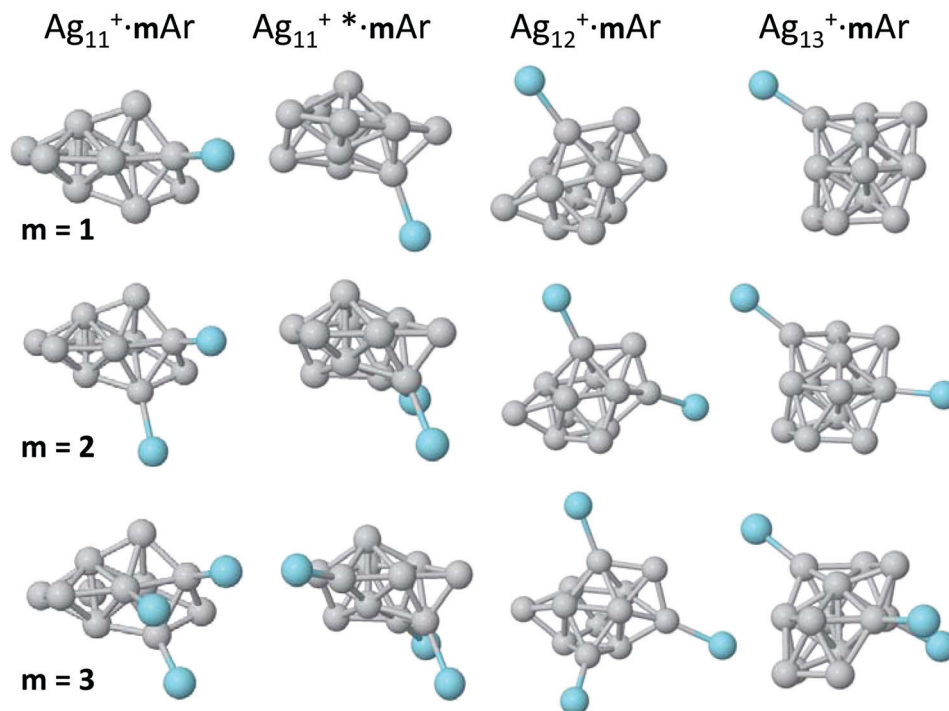
Fig. 2 Lowest energy equilibrium geometry of $Ag_n^+ \cdot m$Ar complexes for $m = 1$ (first row), $m = 2$ (second row), and $m = 3$ (third row). The first and second columns correspond, respectively, to adsorption of Ar on the lowest energy isomer of Ag_{11}^+, and on the near degenerate Ag_{11}^+* isomer (see Fig. 1). The third and fourth columns correspond to Ar adsorption on the lowest energy isomer of Ag_{12}^+, and Ag_{13}^+, respectively.

Table 2 Adsorption energy (see eqn (7)), average distance Ar–Ag, coordination ratio, and charge accumulated on the Ar atoms, for 1 Ar/2 Ar/3 Ar atoms adsorbed on Ag_{11-13}^+ clusters (see Fig. 2). The site coordination ratio given in column four is defined as the quotient of the coordination of the adsorption site with the average coordination of the cluster substrate given in Table 1. In the last column is given the effective physisorption energy density, defined in eqn (9), where the values of $\langle coor \rangle$ and $\bar{\alpha}$ are taken from Table 1

Compound	E_{ads} (eV)	$\bar{d}_{Ar-Ag}$ (Å)	Coor. ratio	Charge ($|e|$)	E_{ads}^{eff} (eV Å^{-3})
$Ag_{11}^+ \cdot$Ar	0.071	3.155	0.868	−0.012	0.493
$Ag_{11}^+ \cdot$2Ar	0.067	3.173	1.013	−0.022	
$Ag_{11}^+ \cdot$3Ar	0.115	3.297	0.965	−0.015	
$Ag_{11}^+* \cdot$Ar	0.070	3.135	0.917	−0.013	0.477
$Ag_{11}^+* \cdot$2Ar	0.076	3.137	0.764	−0.013	
$Ag_{11}^+* \cdot$3Ar	0.080	3.127	0.713	−0.040	
$Ag_{12}^+ \cdot$Ar	0.062	3.185	0.500	−0.010	0.563
$Ag_{12}^+ \cdot$2Ar	0.049	3.210	0.750	−0.017	
$Ag_{12}^+ \cdot$3Ar	0.067	3.183	0.750	−0.030	
$Ag_{13}^+ \cdot$Ar	0.074	3.090	1.026	−0.016	0.525
$Ag_{13}^+ \cdot$2Ar	0.083	3.126	1.197	−0.021	
$Ag_{13}^+ \cdot$3Ar	0.086	3.153	1.140	−0.029	

(An exception is the distance Ar–Ag in $Ag_{11}^+ \cdot$3Ar, which can be related to the positive charging of the third Ar atom already commented on above.) In addition, the coordination ratio is also smaller for the $n = 12$ complexes. On the other hand, we know from mass espectrometry experiments[2] that the capability of Ag_{12}^+ to adsorb Ar atoms is larger than that of neighbor clusters. Since the calculated binding energies of the $n = 12$ complexes are smaller than those of their neighbours, we can discard chemisorption as the leading interaction of Ar with silver clusters.

A qualitative explanation of the trend of binding energies is that the physisorption interactions between Ar and silver clusters must be governed by dispersion (London type) forces, which are proportional to the polarizability and ionization potential of the Ar atom and silver cluster. The polarizability of Ag_{12}^+ is the smaller one among those for Ag_{11-13}^+ clusters in their ground state (see Table 1), and also the ionization potential of Ag_{12}^+ is the smaller one in that range of sizes. In addition, the dispersion forces depend on the distance between Ar and the silver cluster as d_{Ar-Ag}^{-6}, that is, larger d_{Ar-Ag} distances yield lower interaction energies, as can be seen in Table 1.

A possible explanation of the experimental peak at $n = 12$ observed in the Ar adsorption abundance spectra[2] must rest on

the geometrical features of silver clusters rather than adsorption energies and local electronic effects. Bréchignac and coworkers[2] have suggested that the coordination number of the surface atoms may be used as a measure of the interaction between rare gases and silver clusters. On one hand, the calculated average coordination number of Ag_{12}^+ is larger than that of the neighbour clusters, that is, more Ag atoms in a volume unit interact with Ar atoms. On the other hand, recall that the mean polarizability of a molecule represents somehow the effective volume of the electron cloud. Thus, the product of binding energy times the average coordination, divided by the mean polarizability:

$$E_{ads}^{eff} = E_{bind} \times \langle coor \rangle / \bar{\alpha} \qquad (9)$$

represents an effective interaction per volume unit of Ag_n^+ silver clusters with Ar atoms. That effective interaction is given in the last column of Table 2, and it is higher for Ag_{12}^+ than for its neighbours, pointing to Ag_{12}^+ as the more effective cluster in the range $n = 11$–13 for Ar physisorption, which agrees with the experimental facts. In adition, the polarizability asymmetry is smaller for Ag_{12}^+, that is, the dispersion forces are less dependent on the mutual orientation between Ar and the silver cluster.

On the other hand, previous calculations for small cationic silver clusters suggest that rare gases prefer corner and edge adsorption sites.[12] We observe in Table 2 that the coordination ratio of the adsorption site is clearly smaller for Ag_{12}^+ than for its neighbour clusters, that is, corners and edges are preferred.

In this way, occupation of low coordination sites should increase the average coordination of available physisorption sites, and then the factor $\langle coor \rangle / \bar{\alpha}$, which is multiplied by the adsorption energy to obtain the effective physisorption energy density of a given $Ag_n^+ \cdot mAr$ ($m = 0, 1, 2, \ldots$) complex, also increases.

In summary, both experimental facts, the Ar absorption peak at $n = 12$ and the preference for corner and edge adsorption sites, are related, according to our calculations, to odd–even geometrical and electronic effects of $Ag_{11–13}^+$ clusters, namely (i) the differences in their geometrical motifs (pentagonal bipyramid for odd-n and triangular prism for even-n), and (ii) to the effective volume of their electron clouds as given by their dipole polarizabilities.

3.3 Physisorption of one and two N_2 molecules

It is well known that the N_2 molecule is unreactive toward most reagents because of its strong triple bond, large HOMO–LUMO gap, and nonpolarity. Recently, several experimental and theoretical studies about the reactivity in the gas-phase of metal clusters with N_2 have been reported, see the recent work of Zhao and coworkers[51] and references therein. Here we focus on the experimental results for the adsorption of N_2 on Ag_n^+ clusters reported by Bréchignac and coworkers,[2] particularly on those with $n = 11$, 12, and 13.

In the first and second columns of Fig. 3 are shown the adsorption geometries of one and two N_2 molecules on the smallest energy configuration of $Ag_{11–13}^+$ clusters and the Ag_{11}^+*
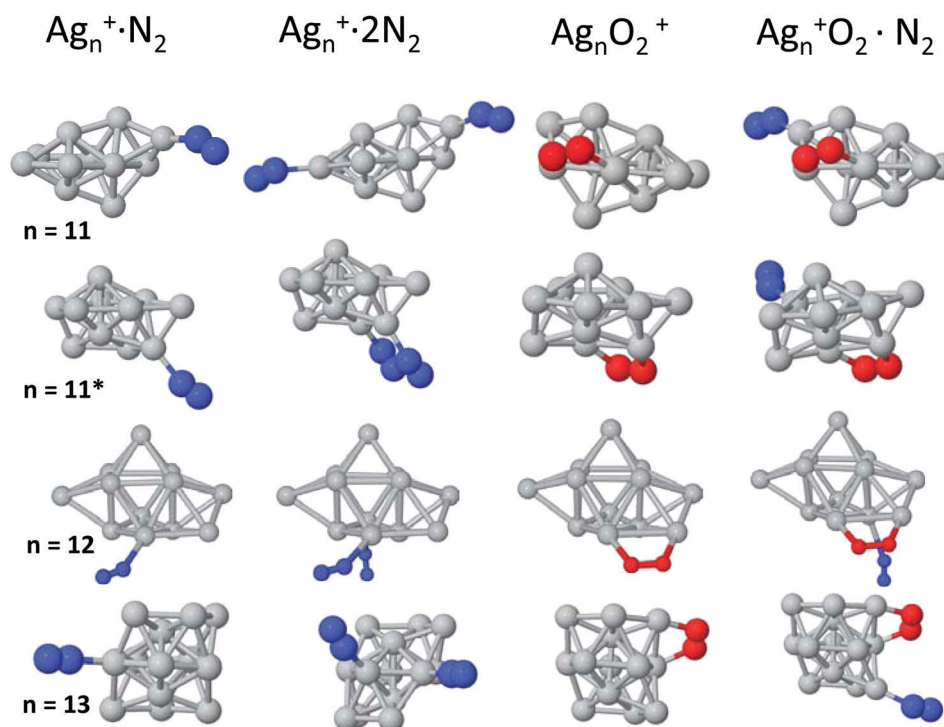

Fig. 3 In the first to third columns are shown the adsorption geometries of N_2, $2N_2$, and O_2 molecules, respectively, on the lowest energy $Ag_{11–13}^+$ clusters and Ag_{11}^+* isomer. The adsorption of O_2 distorts the geometry of the silver clusters, particularly that of Ag_{12}^+. In column four are shown the adsorption geometries of N_2 on the $Ag_n^+O_2$ clusters of the third column.

Table 3 Adsorption energy, bond length of physisorbed N_2, mean distance N_2–Ag, site coordination ratio, accumulated charge on the N_2 molecules, electric dipole moment and mean static dipole polarizability per atom for one and two molecules adsorbed on Ag_{11-13}^+ clusters with the smallest energy geometry and isomer $Ag_{11}^{+}\star$ (see the first and second columns of Fig. 3). The site coordination ratio is defined as the quotient of the coordination of the adsorption site with the average coordination of the silver cluster given in Table 1

Complex	E_{ads} (eV)	d_{N-N} (Å)	$\bar{d}_{N_2-Ag}$ (Å)	Coord. ratio	Charge ($\lvert e\rvert$)	H–L gap (eV)	$\lvert\mu\rvert$ (Debye)	$\bar{\alpha}/n$ (Å³)
$Ag_{11}^+\cdot N_2$	0.165	1.129	2.434	0.866	−0.005	0.831	2.350	6.144
$Ag_{11}^+\cdot 2N_2$	1.145	1.130	2.490	0.866	0.013	0.823	1.317	3.123
$Ag_{11}^{+}\star\cdot N_2$	0.174	1.128	2.445	1.220	−0.007	0.839	2.438	5.666
$Ag_{11}^{+}\star\cdot 2N_2$	0.171	1.130	2.416	0.916	0.012	0.783	4.014	7.037
$Ag_{12}^+\cdot N_2$	0.137	1.129	2.497	0.750	−0.006	0.176	2.361	6.543
$Ag_{12}^+\cdot 2N_2$	0.139	1.129	2.502	0.875	−0.009	0.178	2.122	4.274
$Ag_{13}^+\cdot N_2$	0.212	1.129	2.395	1.711	0.002	0.954	2.095	5.720
$Ag_{13}^+\cdot 2N_2$	0.158	1.129	2.439	1.027	0.020	0.946	2.572	6.040

isomer. In Table 3 are given the adsorption energy (see eqn (7)), bond length of physisorbed N_2, average distance of N_2 to the cluster, site coordination ratio, accumulated charge on the N_2 molecules, and HOMO–LUMO gap for the complexes shown in Fig. 3. In the last two columns of Table 3 are given the magnitude of the electric dipole moment and the mean polarizability as defined in eqn (2) and (4), respectively. We see in Fig. 3 that N_2 binds on top of Ag atoms, which is a signal of possible physisorption, because it has been noted experimentally that N_2 physisorption is enhanced in upright positions at edges and corners of charged particles[2,52,53] (in particular nickel and other 3d metal clusters). That feature was also obtained by means of DFT calculations for the adsorption of several N_2 molecules on small Ag_n^+ clusters.[12]

As expected for physisorption interactions, we see in Table 3 that the N–N distance in the adsorbed N_2 does not differ appreciably from that calculated for the free molecule, 1.13 Å. Other signtures of physisorption shown in Table 3 are the small adsorption energies, the large $\bar{d}_{N_2-Ag}$ distances to the Ag substrate (smaller, however, than those $\bar{d}_{Ar-Ag}$ in Table 2), and the small charging of N_2. The charge accumulated on the first and first plus second physisorbed N_2 molecules is given in the sixth column of Table 3, as calculated by means of the Bader method.[50] We see that only for the Ag_{12}^+ cluster do the first and second N_2 adsorbed atoms donate electronic charge to the silver substrate, and just the contrary occurs for Ag_{13}^+. Instead, the first adsorbed N_2 donates electronic charge to Ag_{11}^+ and $Ag_{11}^{+}\star$ and the second adsorbed N_2 accepts electronic charge from the silver substrate. Thus, N_2 can be considered as an amphoteric species, which either donates or accepts electrons from metal species.

The smallest adsorption energy, the largest $\bar{d}_{N_2-Ag}$ distance, and the smallest coordination ratio in Table 3 correspond to $Ag_{12}^+\cdot mN_2$. As these features also appear for $Ag_{12}^+\cdot mAr$ (see Table 2), one is tempted to assume an analogous explanation of the observed peaks in the abundance spectra of N_2 and Ar adsorption on Ag_n^+ clusters. However, the N_2 adsorption energies are more than two times larger than those for Ar adsorption, although still they are about one order of magnitude smaller than those of typical covalent interactions (see the binding energies of Ag atoms in Table 1). In addition, the $\bar{d}_{N_2-Ag}$

distances are ∼0.8 Å smaller than the $\bar{d}_{Ar-Ag}$ distances. Thus, although the physisorption mechanism based on (London) dispersion forces (used above to rationalize the Ar adsorption energies) may also explain the trend of the N_2 adsorption energies, the full interaction of N_2 with Ag_n^+ clusters must involve other components, like a dipole-induced dipole mechanism (Debye forces), or, more probably, a non-covalent mechanism based on π–π or cation–π interactions. That cation–π interaction is surprisingly strong,[44] and could explain the exceptional adsorption energy of N_2 on $Ag_{11}^+\cdot N_2$. π–π interactions are associated with the overlap between the π-orbitals of a molecular system. With respect to the 4d electrons of silver we recall that the s–d promotion energy in the valence region is much higher than that for copper and gold condensates, because the eigenvalues of the s (d) valence electrons of silver are less (more) deeply bound than their counterparts of copper and gold. Thus, the participation of 4d electrons in the frontier orbitals and bonding of silver clusters with ligands like N_2 is less important than that of the s and p components.

In order to better understand the bonding character of nitrogen molecules to silver clusters we discuss now the orbital projected density of states (PDOS) of $Ag_n^+\cdot mN_2$ complexes with n = 11–13 (including $Ag_{11}^{+}\star$) and m = 0, 1, 2, which is presented in Fig. 4 and, with a focus around the Fermi level, in Fig. 5. First we can distinguish in all cases a region between −6.0 and −2.5 eV delimited and dominated by the 4d orbital of Ag. The PDOS of that big 4d peak at these energies is presented only between −5.0 a.u. and 5.0 a.u. to allow us to display details of the other components. In that region of energy there is a net hybridization of the 4d orbital with the 5s and 5p orbitals of Ag, having nearly the same shape in all the cases. The exception is $Ag_{12}^+\cdot mN_2$, whose PDOS shows a small difference with the other aggregates for all m values, probably due to its different structural motif. The PDOS of 2s, 2p, and 3d of nitrogen in the region between −6.0 eV and −2.5 eV is shown with more detail in Fig. 5, where we can see that $Ag_{12}^+\cdot mN_2$ (m = 1, 2) shows two lobes instead of the three lobes shown by the other aggregates. The region below −7.0 eV is dominated by the orbitals 2s, 2p, and 3d of nitrogen, and their shapes do not change (only the amount of charge) after the adsorption of the second N_2 (except, slightly, for $Ag_{13}^+\cdot 2N_2$). On the other hand, in the region of positive energies larger than 1 eV (see Fig. 4),

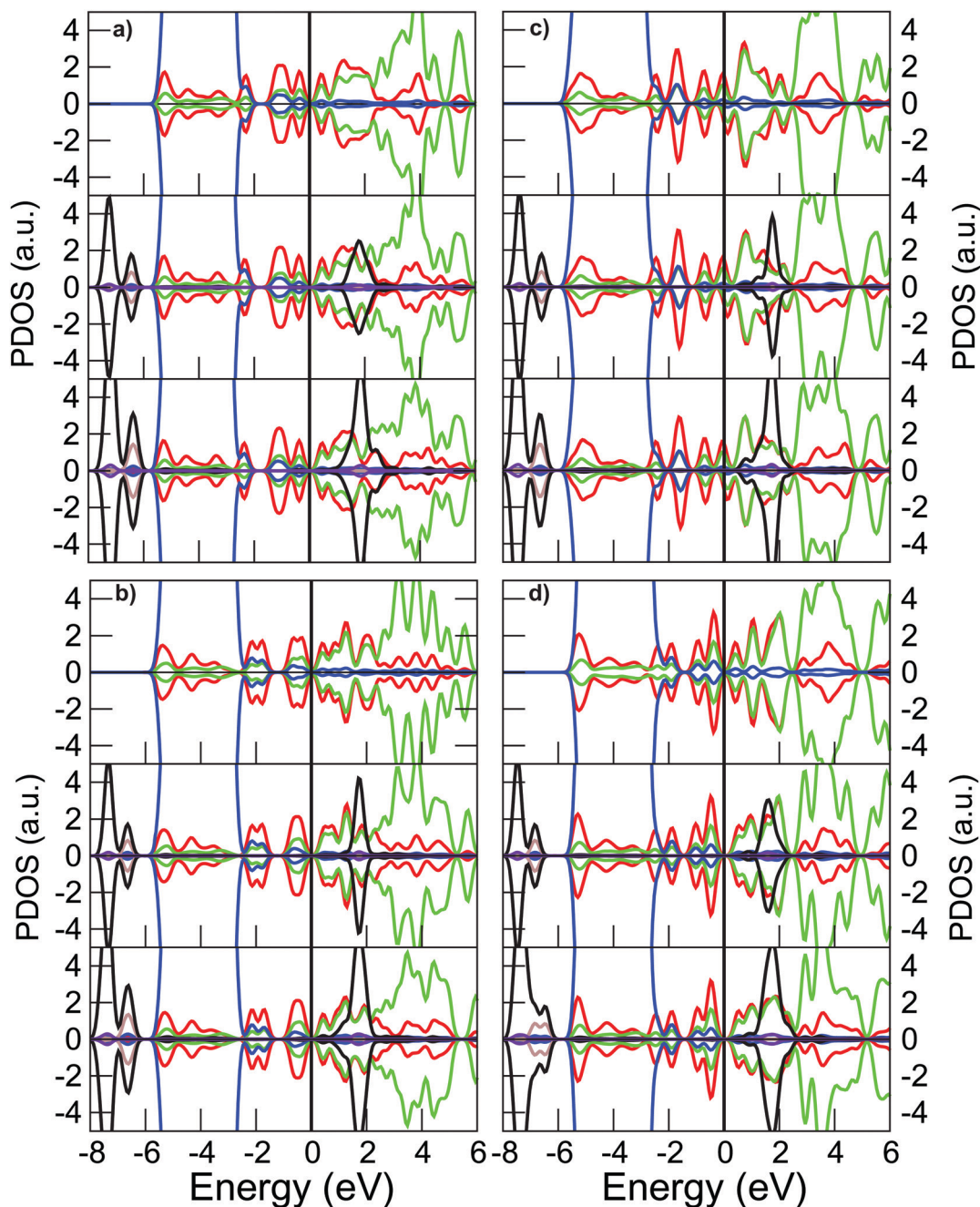**Fig. 4** The spin-up and spin-down orbital projected density of states (PDOS) of $Ag_n^+ \cdot mN_2$ complexes ($m = 0, 1, 2$) for (a) $n = 11$; (b) $n = 11^*$; (c) $n = 12$; and (d) $n = 13$. In each of these panels are given the three compounds: $m = 0$ (top), $m = 1$ (medium), and $m = 2$ (bottom). The projections on orbitals 5s, 5p, and 4d of Ag are represented by the colors red, green, and blue, respectively, and the orbitals 2s, 2p, and 3d of N are represented by the colors brown, black, and violet, respectively. The Fermi energy has been set to zero in all the cases.

the more distinctive feature of the PDOS is the higher peak at ≈ 2 eV for the 2p orbital of nitrogen, which, in the case of $Ag_{11}^+ \cdot 2N_2$, extends beyond 2 eV to fully hybridize with a 5s lobe of silver. That feature may contribute to the extra stabilization of the $Ag_{11}^+ \cdot 2N_2$ cluster.

The more interesting differences in the PDOSs of $Ag_n^+ \cdot mN_2$ clusters shown in Fig. 4 appear between -2.5 eV and 2.5 eV, around the Fermi level (set at zero energy). Just each side of the Fermi energy, Ag_{12}^+ has occupied (spin up) and unoccupied

(spin-down) 5s, 5p, and 4d orbitals (top panel (c)) which hybridize with 2s, 2p, and 3d orbitals of nitrogen, respectively, when forming $Ag_{12}^+ \cdot mN_2$ (medium and bottom panels of (c)). That can be seen in more detail in both panels (c) of Fig. 5. That feature, which is unique to $Ag_{12}^+ \cdot mN_2$ (due to the spin multiplicity 2 of Ag_{12}^+), is the signature of its enhanced reactivity. In other words, the smaller HOMO–LUMO gap of $Ag_{12}^+ \cdot mN_2$ with respect to their odd-n neighbours (see Tables 1 and 3) explains the higher reactivity of Ag_{12}^+ toward N_2 as compared with its neighbours.
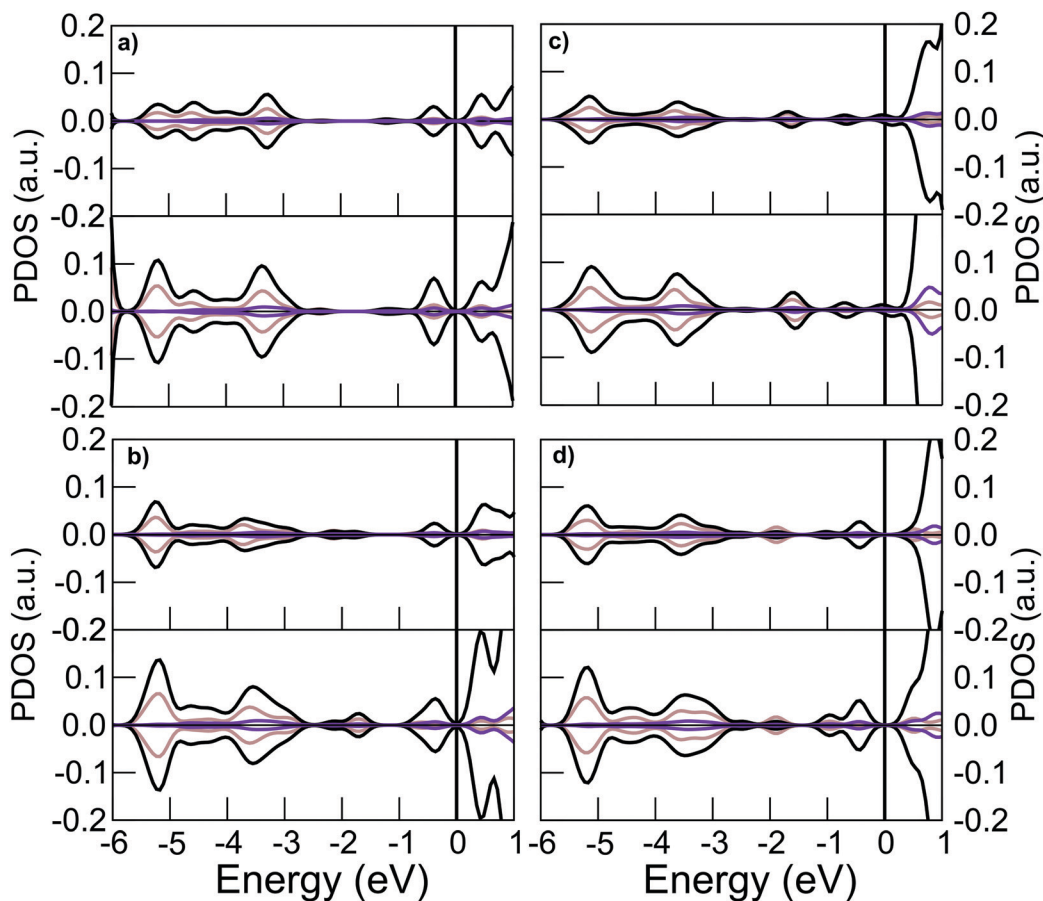
Fig. 5 The same as Fig. 4, excluding the $m = 0$ case (pure silver cluster), is represented, for the sake of clarity, in a smaller vertical interval, and only the PDOS of 2s (brown), 2p (black), and 3d (violet) orbitals of nitrogen are shown.

Concerning $Ag_{11}^+* \cdot mN_2$, there is a difference with respect to the PDOS of the other clusters in the region between -2.5 eV and the Fermi energy, showing two lobes of hybridization between the 5s and 5p orbitals of Ag, instead of three lobes. Finally, the origin of the extraordinary adsorption energy of N_2 on $Ag_{11}^+ \cdot N_2$ with respect to the other N_2 complexes studied here may be the higher overlap between the silver and nitrogen orbitals, as can be seen in the bottom panel of Fig. 4(a) and of Fig. 5(a) compared to its analogous PDOS in the other panels.

As said in the previous subsection, mass spectrometry experiments[2] show analogous adsorption patterns for Ar and N_2 molecules on Ag_{2-20}^+ clusters, including a notorious peak at Ag_{12}^+ superimposed on the general decreasing trend with size. For both the Ar and N_2 cases, that peak is due to dispersion London interactions yielding an effective adsorption energy density which is larger for $n = 12$ than for its neighbour clusters. In addition, for N_2 the non-covalent $\pi-\pi$ interactions between N_2 and the silver cluster must be considered, which are favored by the small HOMO–LUMO gap of Ag_{12}^+. Note that the adsorption of the first N_2 tends to narrow (enlarge) the HOMO–LUMO of the pure silver clusters with odd-n (even-n), and the adsorption of the second N_2 produces the same effect.

We analyze now the magnitude and direction of the dipole moments. The magnitude of $|\mu|$ for clusters with an adsorbed N_2 molecule does not show special variation with size, having values in the range 2.10–2.44 Debye. After adsorbing a second N_2, only the dipole moment of $Ag_{11}^+ \cdot 2N_2$ and of $Ag_{11}^+* \cdot 2N_2$ changes significantly (decreasing and increasing, respectively). That is due, in both cases, to the orientation of the second N_2 molecule with respect to the first one, resulting in opposite and parallel directions, respectively (see Fig. 3). These relative orientations lead to very different dipole–dipole energy, which should be reflected in some way in the total binding energy.

Concerning the mean dipole polarizability, we already noted that Ag_{12}^+ has the smaller one in the range $n = 11$–13 (and slightly larger than that of the Ag_{11}^+* isomer, see Table 1). This fact, according to the empirical rule that the higher the polarizability the higher the stability,[47,54] points to Ag_{12}^+ as the less stable (more reactive) cluster towards N_2 physisorption in the range $n = 11$–13. On the other hand, the values of the mean polarizability of $Ag_n^+ \cdot N_2$ complexes in Table 3 are higher than those of the Ag_n^+ clusters. According to the above mentioned empirical rule, $Ag_n^+ \cdot N_2$ are more stable (less reactive) than Ag_n^+ clusters, which agrees with the observed competitivity of N_2 adsorption on cationic silver clusters.[2,12]

3.4 Chemisorption of O$_2$

According to classical arguments,[2] the chemisorption energy of electron acceptors (like O_2) on positively charged large clusters

should increase as the cation size increases, because the electrical capacitance also increases and then the extractable charge increases. Nevertheless, superimposed local effects, both electronic and geometrical, strongly interfere with these trends, as observed for Ag_n^+ clusters with n up to 40 atoms.[2,5,12] As a mater of fact, it has been observed no more than one O_2 molecule on Ag_n^+ clusters with $n < 22$. In mass spectrometry experiments,[2] a clear peak for $Ag_{12}^+O_2$ was observed.

In the third column of Fig. 3 are shown the lowest energy configurations of $Ag_n^+O_2$ clusters. The O_2 molecule is always adsorbed in the bridge position, causing a slight modification of the substrate geometry. Other DFT calculations for the oxidation of neutral and anionic silver clusters[6,10] predict that O_2 adsorbs on top of Ag atoms (e.g., neutral Ag_{13} and anionic Ag_{11}^- and Ag_{13}^-).

The O_2 adsorption mechanism on noble metal clusters (neutral and charged) is based on the frontier orbital model.[55–57] The degenerate $2p\pi_g*$ anti-bonding orbitals of O_2 are each occupied by an unpaired electron forming a triplet open-shell electronic structure. That structure acts as an electron acceptor when interacting, through oxidative adsorption, with the electron in the highest occupied orbital (HOMO) of a noble metal cluster, which has σ-type symmetry. This mechanism is similar to that found in the adsorption of NO, to be discussed later through the detailed analysis of the orbital projected density of states.

In Table 4 are given the adsorption energy, bond length of chemisorbed O_2, average distance of O_2 to the silver substrate, average local coordination ratio, and charge of the O_2 molecule adsorbed on $Ag_{11–13}^+$ clusters (including Ag_{11}^{+*}). There is a positive correlation between the calculated adsorption energies and the abundance of $Ag_n^+O_2$ clusters observed in the mass spectrum,[2] which shows a clear peak at $n = 12$. This correlation, as well as the high O_2 adsorption energies when compared with those of Ar and N_2, points to typical oxidative chemisorption, Ag_{12}^+ being more reactive than its neighbour clusters. The bond length of adsorbed O_2 is always larger than that in the free molecule (1.22 Å), in particular when adsorbed on Ag_{12}^+. At $n = 12$, the distance between the O_2 molecule and the silver cluster is a minimum and the charge of O_2 is a maximum, which allows one to characterize the state of that adsorbed molecule as a superoxide. Certainly, this can be described as weak chemisorption, in comparison with the much higher adsorption energies and charge transfer of O_2 on neutral and anionic silver clusters reported in the literature. From Bader charge analysis, it can be seen that the $0.5e^-$ gained by the O_2

molecule is provided by the two Ag atoms which bind to the oxygen in the bridge position. The charge hole does not change and the structure of Ag_{12}^+ remains unaltered practically.

The observed odd–even alternation in reactivity (abundance) of $Ag_{11–13}^+$ clusters towards O_2 can be rationalized in terms of the frontier orbital model for O_2 adsorption. In the case of $n = 12$, the HOMO of Ag_{12}^+ has an unpaired electron and a relatively low HOMO–LUMO gap, such that the electron can be easily paired with the single electron in one π_g* orbital of O_2. It results in an attractive interaction and large partial electron transfer to the O_2 adsorbate. In contrast, for odd n cationic clusters, the HOMO is doubly occupied leading to a higher HOMO–LUMO gap and smaller electron transfer to the adsorbate. It results in a less attractive interaction with the O_2 π_g*, because the additional electron must be placed in the antibonding orbital of the $Ag_n^+O_2$ complex. Thus, the HOMO–LUMO gap of odd-n (even-n) Ag_n^+ clusters becomes smaller (larger) after adsorption of O_2, resulting in the HOMO–LUMO gap of Ag_{12}^+ evolving from a minimum to a maximum value. A similar effect was noted for the sequential adsorption of one and two N_2 molecules. We will further comment on the HOMO–LUMO gap in the next two subsections, when comparing these values with those of $Ag_n^+O_2N_2$ and Ag_n^+NO aggregates.

3.5 Cooperative adsorption of N_2 and O_2 on Ag_n^+ ($n = 11$–13)

Simultaneous chemisorption of identical molecules on small clusters should be competitive because the electrical capacitance (and then the extractable charge) is limited by the finite size of the cluster. As said before, no more than one O_2 molecule chemisorbed on Ag_n^+ has been observed in the range $n < 22$.[2] However, coadsorption of donors with acceptors can be cooperative because the donor chemisorption promotes the reaction with the acceptor through the mechanism of shifting the electron affinity (or ionization potential) and vice versa. Such indirect charge transfer has been studied previously in metal clusters[57,58] and surfaces.[59]

In the fourth column of Fig. 3 are shown the minimum energy configurations of N_2 adsorbed on $Ag_{11–13}^+O_2$ and $Ag_{11}^{+*}O_2$. We see that the presence of O_2 changes the adsorption site of N_2 on the nude silver cluster, except for $n = 11$ (compare the first and fourth columns of Fig. 3). In Table 5 are given the adsorption energy of N_2 on $Ag_{11–13}^+O_2$, the bond lengths of chemisorbed O_2 and physisorbed N_2, the distances O_2–Ag and N_2–Ag, the coordination rate of N_2 and O_2 adsorption sites, the charge of O_2 and N_2 molecules adsorbed on $Ag_{11–13}^+$ clusters, and the HOMO–LUMO gap. All the values in

Table 4 Adsorption energy, E_{ads} (eV), bond length of chemisorbed O_2 (Å), average distance of O_2 to the silver substrate, average site coordination ratio, charge of the O_2 molecule adsorbed on $Ag_{11–13}^+$ clusters (see the third column of Fig. 3) and HOMO–LUMO gap. The O_2 molecule is always adsorbed in the bridge position, with slight modification of the substrate geometry. The coordination ratio is defined as the quotient of the average coordination of the bridged Ag atoms with the average coordination of the silver cluster given in Table 1

Cluster	E_{ads} (eV)	d_{O-O} (Å)	$\bar{d}_{O_2-Ag}$ (Å)	⟨Coord. ratio⟩	Charge ($|e|$)	H–L gap (eV)
$Ag_{11}^+O_2$	0.342	1.303	2.403	1.013	0.341	0.306
$Ag_{11}^{+*}O_2$	0.417	1.312	2.339	0.916	0.377	0.243
$Ag_{12}^+O_2$	0.746	1.343	2.267	0.875	0.506	0.347
$Ag_{13}^+O_2$	0.357	1.299	2.395	1.197	0.325	0.279

Table 5 Adsorption energy of N_2 on $Ag_{11-13}^+O_2$ (column 2), bond lengths of adsorbed O_2 and N_2 (column 3), average distances O_2–Ag and d_{N_2-Ag} (column 4), coordination ratio of O_2 and N_2 (column 5), charge of adsorbed O_2 and N_2 molecules (column 6), and HOMO–LUMO gap (column 8). The O_2 (N_2) molecule always adsorbs on bridge (atop) sites, as shown in Fig. 3, without noticeable modification of the substrate geometry

Complex	E_{ads} (eV) of N_2	d_{O-O} (Å) d_{N-N} (Å)	d_{O_2-Ag} (Å) d_{N_2-Ag} (Å)	O_2 coord. N_2 coord.	O_2 charge ($|e|$) N_2 charge ($|e|$)	H–L gap (eV)
$Ag_{11}^+O_2 \cdot N_2$		1.303	2.398	1.013	0.345	0.305
	0.175	1.129	2.417	0.868	−0.005	
$Ag_{11}^{+*}O_2 \cdot N_2$		1.314	2.328	0.916	0.384	0.227
	0.155	1.129	2.487	1.528	−0.004	
$Ag_{12}^+O_2 \cdot N_2$		1.344	2.264	0.875	0.512	0.616
	0.115	1.128	2.661	0.750	−0.008	
$Ag_{13}^+O_2 \cdot N_2$		1.300	2.403	1.197	0.329	0.279
	0.175	1.129	2.424	1.368	−0.009	

Table 5 were obtained optimizing all posible configurations of N_2 adsorbed on the lowest energy $Ag_n^+O_2$ compound obtained previously. Notice that the (small) rearrangement of all the atom–atom distances after optimization of the complexes may affect the local coordination values, as well as the other structural magnitudes.

The adsorption energy and N–N bond length values of N_2 on $Ag_n^+O_2$ are small and comparable to those for adsorption on pure Ag_n^+ clusters, which points to a similar N_2 adsorption mechanism on pure and oxidized cationic silver clusters, that is, based on dispersion forces plus p–p (or cation–p) interactions. Similarly, the charging of N_2 on both substrates is very small. The very modest increase of the electronic charge of O_2 in $Ag_n^+O_2 \cdot N_2$ with respect to that in $Ag_n^+O_2$ is provided mainly by the silver substrate.

On the other hand, the enhancement of O_2 chemisorption by the presence of physisorbed N_2 has been observed.[2,58] This effect was qualitatively explained assuming that the negative charge of the dipoles on the N_2 surface partly compensates the positive charge of the cluster, which facilitates the charge transfer to oxygen. That is, the nitrogen acts as a dielectric that enhances the capacitance of a small capacitor. Thus, the extraction of negative charge is easier and chemisorption of oxygen becomes enhanced. We have not studied this effect in this paper.

More indicative of the cooperative conjoint adsorption of O_2 and N_2 is the trend with size n in the change of the HOMO–LUMO value from Ag_n^+ to $Ag_n^+O_2$ and $Ag_n^+O_2 \cdot N_2$ complexes. The adsorption of O_2 reduces (increases) the HOMO–LUMO of odd-n (even-n) Ag_n^+ clusters, turning the minimum value at Ag_{12}^+ into a maximum HOMO–LUMO for $Ag_{12}^+O_2$. Thus, the even-n

cluster is stabilized with respect to the odd-n clusters after O_2 adsorption. The subsequent adsorption of N_2 on $Ag_n^+O_2$ leaves practically unaltered the HOMO–LUMO gap of aggregates with odd n, but in the case of $n = 12$ the HOMO–LUMO becomes nearly twice, stabilizing further that aggregate with respect to its neighbours. This effect was not obtained for the second N_2 adsorption on $Ag_n^+N_2$. In this sense, we can say that N_2 and O_2 are cooperatively adsorbed on Ag_n^+ clusters. Interestingly, the consecutive adsorption of O_2 and N_2 on Ag_n^+ clusters switches their semiconductor character from low (high) HOMO LUMO in even-n (odd-n) towards the opposite behavior. This fact may be used, in principle, to implement a sensor of increasing presence of N_2 gas.

3.6 Chemisorption of NO

NO_x is produced in fuel combustion engines, and its reduction to nitrogen is crucial in reducing air pollution. It is known that NO adsorbs on the bridge site of Au(100), which ensures efficient overlap of the NO π^* orbital with the orbitals of the two neighbouring noble metal atoms, and with the NO bond axis aligned along the surface normal.[60] In a recent DFT study of NO adsorption on M_n neutral clusters (M = Ru, Rh, Pd, Ag; n = 13, 55),[61] it is concluded, by analyzing the PDOS of M_nNO and the charge transfer between NO and M_n, that NO dissociative adsorption occurs on M = Ru and Rh, molecular NO adsorption occurs on M = Pd, and NO dimerization occurs on M = Ag. The reactions of NO with $Ag_n^\pm$ clusters in the gas phase with n = 7–69 have been studied experimentally by Ma and coworkers[11] using a continuous flow reactor running at low temperatures. These authors conclude that the interactions are dominated by electron transfer from silver to NO. In the region
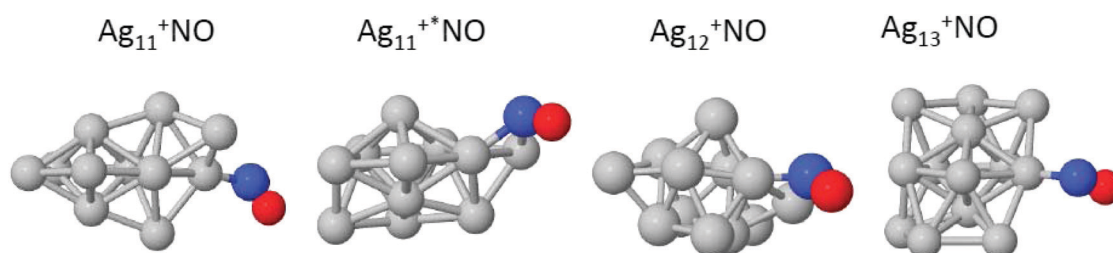

Fig. 6 Lowest energy configuration of NO adsorbed on Ag_{11-13}^+ clusters.

of sizes n = 11–13 which we are considering here, these experiments shows a small signal of dissociation of NO at n = 12, as well as the production of the new product $Ag_{12}NO_2{}^+$. The molecular adsorption of the first NO is enhanced at low temperatures because it is generally a barrierless process. In the following we study only the non dissociative adsorption of NO on $Ag_{11-13}{}^+$ clusters, in order to learn about the mechanism of adsorption in comparison with the adsorption of O_2. Further work about the NO dissociation mechanism is in progress.

In Fig. 6 is shown the lowest energy configuration of NO adsorbed on the minimum energy structure of $Ag_{11-13}{}^+$ clusters and on the $Ag_{11}{}^{+*}$ isomer. The N species of NO is always the closest to the cluster, and the adsorption site is on top of Ag for n = 11 and 13, and bridging two Ag atoms for n = 12 and for the $Ag_{11}{}^{+*}$ isomer. The molecular axis of NO orients nearly perpendicular to the dipole moment of the cluster (see Fig. 1) in order to maximize the overlap of the $\pi_z{}^*$ orbital of NO with the 5s–5p orbitals of silver clusters. The resulting dipole moments

of $Ag_n{}^+NO$ and those of $Ag_n{}^+$ (shown in Fig. 1) form angles of $105.00°$, $64.87°$, $172.16°$, and $0.88°$, respectively, for n = 11, 11★, 12, and 13. Thus, after NO adsorption, the $Ag_{12}{}^+NO$ molecule orients its dipole moment in (nearly) the opposite direction to that of $Ag_{12}{}^+$, whereas the $Ag_{13}{}^+NO$ molecule orients its dipole moment in (nearly) the same direction as the $Ag_{13}{}^+$ moment.

In Table 6 are given the adsorption energy, bond length, distance of NO to the silver cluster, average site coordination ratio, charge on the N and O atoms, HOMO–LUMO gap, and modulus of the electric dipole moment for an adsorbed NO molecule on $Ag_{11-13}{}^+$ clusters and the $Ag_{11}{}^{+*}$ isomer. There is a clear peak of the adsorption energy for $Ag_{12}{}^+$, which is due to the odd number of electrons leading to a smaller HOMO–LUMO gap (see Table 1) than its neighbour clusters, and then to higher reactivity. This is also consistent with the larger N–O distance (pre-dissociation), smaller distance of NO to the cluster, larger dipole moment, and higher charging of both N and O for NO adsorption on the n = 12 cluster than for

Table 6 Adsorption energy, bond length of chemisorbed NO, average distance of NO to the nearest Ag atom(s) of the silver cluster, average coordination ratio, charge on the N/O atoms of the NO molecule, HOMO–LUMO gap, and dipole moment of complexes of NO adsorbed on the minimum energy configuration of $Ag_{11-13}{}^+$ clusters and the $Ag_{11}{}^{+*}$ isomer (see Fig. 6)

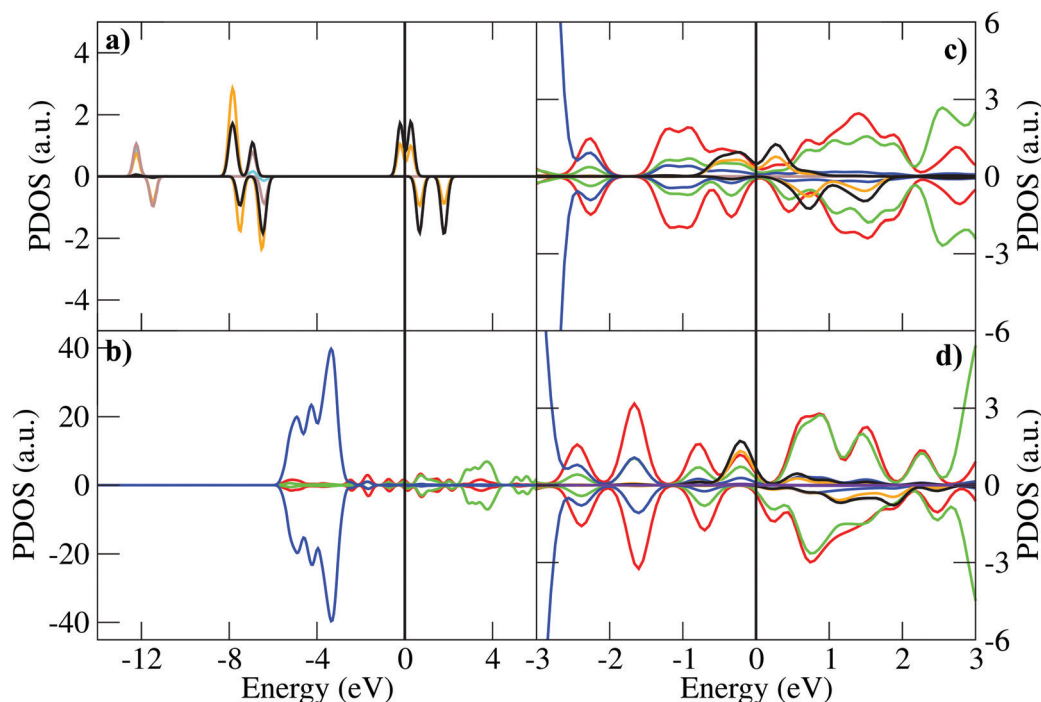| Cluster	E_{ads} (eV)	d_{N-O} (Å)	$\bar{d}_{N-Ag}$ (Å)	Av. coor. ratio	N/O charge ($|e|$)	H–L gap (eV)	$|\bar{\mu}|$ (Debye)
$Ag_{11}{}^+NO$	0.579	1.194	2.206	0.434	−0.193 / 0.297	0.476	4.693
$Ag_{11}{}^{+*}NO$	0.620	1.209	2.398	1.528	−0.073 / 0.292	0.733	4.792
$Ag_{12}{}^+NO$	0.755	1.227	2.323	0.625	0.020 / 0.325	0.392	5.279
$Ag_{13}{}^+NO$	0.624	1.193	2.214	1.026	−0.139 / 0.250	0.535	3.729

Fig. 7 (a) Projected density of states (PDOS) of the NO molecule on the O-2s (light blue), O-2p (orange), N-2s (brown) and N-2p (black) orbitals. (b) PDOS for $Ag_{12}{}^+$ on the 5s (red), 5p (green), and 4d (blue) orbitals. (c) PDOS for $Ag_{11}{}^+NO$ on the 5s, 5p, and 4d of Ag and 2s and 2p for O and N in the region (−3 eV, 3 eV) around the Fermi level. (d) The same as in (c) for $Ag_{12}{}^+NO$. The Fermi level is set at zero energy in all panels. The projections on orbitals 5s, 5p, and 4d of Ag are represented by the colors red, green, and blue, respectively, the orbitals 2s and 2p of O are represented by the colors cyan and orange, and the orbitals 2s and 2p of N are represented by the colors brown and black, respectively. The Fermi energy has been set to zero in all the cases.

adsorption on the ground state of n = 11, 13 clusters. Notice that both the N and O components of NO act as electron acceptors when chemisorbed on Ag_{12}^+. This fact points to Ag_{12}^+ as more favorable for dissociation[11] than for dimerization of adsorbed NO molecules.[61] In addition, the chemisorption at n = 12 occurs by bridging two low coordinated atoms of the silver cation, maximizing the overlap between the (half-filled) π^* frontier orbital of NO and the s and p components of the silver valence configuration of Ag_{12}^+ in the HOMO region.

This way of bonding between NO and Ag_n^+ cations is illustrated in Fig. 7, where the projected density of states (PDOS) on the s, p, and d components has been drawn for the NO molecule (panel a), Ag_{12}^+ (panel b), Ag_{11}^+NO (panel c) and Ag_{12}^+NO (panel d). We see in panel (a) that only the spin-up π^* molecular orbital of NO is occupied at the Fermi level, and in panel (b) we see that the main interaction of NO with Ag_n^+ is the overlapping of that π^* orbital with the 5s and 5p orbitals of the silver cluster. Such hybridization is illustrated in detail in panels (c) and (d) of Fig. 7 for Ag_{11}^+NO and Ag_{12}^+NO, respectively. For Ag_{12}^+NO we see the perfect matching of the spin-up 5s and 5p components of the silver cluster with spin-up 2s and 2p of the NO molecule around the Fermi level, leading to an enhanced binding energy. We also see the absence of spin up and down compensation (contrary to the case Ag_{11}^+NO), which originates the spin multiplicity 3 for the compound Ag_{12}^+NO.

The HOMO–LUMO gap of Ag_{12}^+NO remains smaller than that of its neighbours, and then that aggregate is the more reactive, and it may adsorb more easily another NO molecule, giving dimerization[61] or yielding reactions towards Ag_{12}^+NO$_2$.[11]

4 Conclusions

We have used an accurate non-local correlation van der Waals density functional to study the observed odd–even effects in the abundance spectra of $Ag_{11-13}^+ \cdot m$X complexes,[2] formed after adsorption and coadsorption of one or more X = Ar, N$_2$, O$_2$, and NO adsorbates on cationic silver clusters Ag_{11-13}^+, with sizes in the 3D^s (s = 2–4) non-closed shell region of metal clusters. We have addressed the explanation of the following experimental facts. For X = Ar, N$_2$, and O$_2$ reactions with Ag_{11-13}^+ an abundance peak at n = 12 was observed.[2] In addition competition between adsorption of two or more N$_2$ was observed, and the cooperative effect of N$_2$ together with O$_2$ adsorption. For X = NO, an abundance peak at n = 12 was also observed,[11] together with a small signal of dissociation and the production of Ag_{12}^+NO$_2$.

Firstly, the optimized geometries of Ag_{11-13}^+ clusters show distinctive motifs in their generation, depending on an odd or even number of atoms. That motif is a pentagonal bipyramid for odd n and a triangular prism for even n. This fact is of relevance to rationalize the geometrical effects in the adsorption of Ar and N$_2$ molecules, which is ruled by physisorption interactions. Our self-consistent calculations with a non local correlation van der Waals density functional describe accurately the electronic interactions in physisorption, particularly the

electric dipole moment and static dipole polarizability, which are important properties in that process. The smallest binding energy and smallest polarizability, but the highest average coordination, were obtained for the Ag_{12}^+ cluster.

The interactions of X = Ar, N$_2$, O$_2$, and NO with Ag_{11-13}^+ clusters, according to the calculated adsorption energies, distances of the adsorbate to the silver cluster, and charge on the adsorbate, may be characterized as non-covalent for Ar and N$_2$, and of the charge transfer type for O$_2$ and NO. In the case of Ar, the process was experimentally characterized as physisorption, and we find that it is ruled by dispersion (London type) interactions. In that process, the geometry (average coordination) and the dipolar polarizability (volume of the electron cloud) of the cluster substrate both play a crucial role. We introduce an effective adsorption energy density, E_{ads}^{eff}, given by the calculated adsorption energy times the average coordination number and divided by the dipole polarizability. It results that the higher E_{ads}^{eff} corresponds to Ag_{12}^+, which is also the cluster with the higher capability for Ar adsorption in that region of cluster sizes, according to mass spectrometry experiments.[2] For the sequential adsorption of up to three Ar atoms, we obtain that Ar atoms always adsorb on top of Ag atoms. The first adsorbed Ar on Ag_{12}^+ prefers the local site with smaller coordination, which increases the average coordination of the available Ag atoms and, thus, increases the capability of the $Ag_{12}^+ \cdot$Ar complex to adsorb more Ar atoms. That explain the prominence of the peak at n = 12 observed in the physisorption of multiple Ar atoms.

The physisorption of one and two N$_2$ molecules is also ruled by dispersion forces, as it is for Ar. However, because the adsorption energy is more than twice higher than that of Ar, the non covalent π–π interaction plays an important role. All that is revealed by the analysis of the PDOS of $Ag_n^+ \cdot m$N$_2$ complexes, and the calculated values of the charging on N$_2$, distances N$_2$–Ag and N–N, HOMO–LUMO gap, and dipole polarizability of $Ag_n^+ \cdot m$N$_2$ complexes. As for Ar, the more abundant N$_2$ adsorption in the region n = 11–13 occurs at Ag_{12}^+ due to its narrow HOMO–LUMO gap and higher overlapping of spin up π-orbitals from the silver cluster with π-orbitals of N$_2$. On the other hand, whereas Ag_{12}^+ has the smaller polarizability (that is, smaller stability according the empirical rule of Ghosh and coworkers[47,54,62]), the complex $Ag_{12}^+ \cdot$N$_2$ has the higher polarizability, and thus the higher stability, hindering the adsorption of a second N$_2$. That feature explains the competition between N$_2$ adsorbates on Ag_n^+ clusters.

With respect to O$_2$ and NO chemisorption on Ag_n^+ clusters, both proceed along the well known charge donation from the silver cluster substrate toward the more electronegative adsorbates. The more reactive cluster is again Ag_{12}^+ due to its smaller HOMO–LUMO gap (and unpaired electron HOMO structure). The O$_2$ adsorption proceeds, according to the frontier orbital model, by accepting charge from the HOMO of the silver cluster to partially fill the degenerate 2pπ^* anti-bonding orbitals of O$_2$ (each one occupied by an unpaired electron, forming a triplet open shell structure). The adsorption of O$_2$ reduces (increases) the HOMO–LUMO of odd-n (even-n) Ag_n^+ clusters, turning its

minimum value at $n = 12$ to a maximum HOMO–LUMO for $Ag_{12}^+O_2$.

Comparing the adsorption energy of N_2 on Ag_n^+ with that on $Ag_n^+O_2$ we see that the adsorption energy slightly decreases in the oxidized clusters (except for $n = 11$), and the charging of N_2 is similar in both cases (except for $n = 13$). Thus, we assume that the N_2 bonding mechanism is similar for Ag_n^+ and $Ag_n^+O_2$. The major differences occur in the trend of the HOMO–LUMO values. The adsorption of N_2 on $Ag_n^+O_2$ nearly maintains the HOMO–LUMO gap of odd-n aggregates but it results twice the HOMO–LUMO in the case of $n = 12$ (which stabilizes that aggregate with respect to its neighbours against further N_2 adsorption). The consecutive adsorption of O_2 and N_2 on Ag_n^+ clusters switches their semiconductor character from low (high) HOMO LUMO for even-n (odd-n) values towards the opposite behavior. Thus, $Ag_{12}^+O_2$ is stabilized by the cooperative adsorption of N_2.

In the case of NO adsorption, the favoured cluster is again Ag_{12}^+ for similar reasons to O_2 chemisorption. The adsorption mechanism is illustrated by examining the projected density of states of $Ag_n^+·NO$ complexes. The HOMO–LUMO gap of Ag_{12}^+NO still is smaller than that of its neighbours, and then more reactive. Thus, that cluster could adsorb another NO molecule, originating dimerization[61] or reactions towards $Ag_{12}^+NO_2$.[11]

Finnally, as an overview about the reactivity trends of Ag_n^+X compounds (X = N_2, O_2, NO) when adsorbed on, for example, TiO_2 surfaces, we extract from our calculations two phenomenological rules, assuming that the HOMO eigenvalue of these compounds may serve as an index of reactivity (R) in such systems:[63]

(i) For all n values, $R(Ag_n^+O_2) > R(Ag_n^+NO) > R(Ag_n^+·N_2)$.

(ii) For a given X (X = N_2, O_2, NO) the reactivity of a compound with $n = 12$ is smaller than that of compounds with $n = 11$ and 13.

Conflicts of interest

The authors declare no competing financial interest.

Acknowledgements

Notes and references

1 J. R. Morones, J. L. Elechiguerra, A. Camacho, K. Holt, J. B. Kouri, J. T. Ramirez and M. J. Yacaman, *Nanotechnology*, 2005, **16**, 2346–2353.

2 M. Schmidt, A. Masson, H.-P. Cheng and C. Bréchignac, *ChemPhysChem*, 2015, **16**, 855–865.

3 B. Sun and A. S. Barnard, *Nanoscale*, 2017, **9**, 12698–12708.

4 Y. D. Kim and G. Ganteför, *Chem. Phys. Lett.*, 2004, **383**, 80–83.

5 L. D. Socaciu, J. Hagen, J. Roux, D. M. Popolan, T. M. Bernhardt, L. Woste and S. Vajda, *J. Chem. Phys.*, 2004, **120**, 2078–2081.

6 E. M. Fernández, M. B. Torres and L. C. Balbás, in *Density functional studies of noble metal clusters. Adsorption of O_2 and CO on gold and silver clusters*, ed. J. P. Julien, J. Maruani, D. Mayou, S. Wilson and G. Delgado-Barrio, Springer, 2006, vol. 15.

7 S. Klacar, A. Hellman, I. Panas and H. Gronbeck, *J. Phys. Chem. C*, 2010, **114**, 12610–12617.

8 Z. Luo, G. U. Gamboa, J. C. Smith, A. C. Reber, J. U. Reveles, S. N. Khanna and A. W. Castleman, *J. Am. Chem. Soc.*, 2012, **134**, 18973–18978.

9 M. Chen, J. E. Dyer, K. Li and D. A. Dixon, *J. Phys. Chem. A*, 2013, **117**, 8298–8313.

10 M.-S. Liao, J. D. Watts and M.-J. Huang, *J. Phys. Chem. C*, 2014, **118**, 21911–21927.

11 J. Ma, X. Cao, H. Liu, B. Yin and X. Xing, *Phys. Chem. Chem. Phys.*, 2016, **18**, 12819–12827.

12 Y.-N. Wu, M. Schmidt, J. Leygnier, H.-P. Cheng, A. Masson and C. Bréchignac, *J. Chem. Phys.*, 2012, **136**, 024314/1–8.

13 G. U. Gamboa, A. C. Reber and S. N. Khanna, *New J. Chem.*, 2013, **37**, 3928–3935.

14 M. L. McKee and A. Samokhvalov, *J. Phys. Chem. A*, 2017, **121**, 5018–5028.

15 T. M. Bernhardt, J. Hagen, S. M. Lang, D. M. Popolan, L. D. Socaciu-Siebert and L. Wöste, *J. Phys. Chem. A*, 2009, **113**, 2724–2733.

16 D. Palagin and J. P. K. Doye, *Phys. Chem. Chem. Phys.*, 2016, **18**, 22311–22322.

17 S. Kohaut and M. Springborg, *J. Cluster Sci.*, 2016, **27**, 913–933.

18 P. L. Rodriguez-Kessler, S. Pan, E. Florez, J. L. Cabellos and G. Merino, *J. Phys. Chem. C*, 2017, **121**, 19420–19427.

19 A. Shayeghi, R. Schäfer, D. M. Rayner, R. L. Johnston and A. Fielicke, *J. Chem. Phys.*, 2015, **143**, 024310.

20 P. V. Nhat, N. T. Si and M. T. Nguyen, *J. Mol. Model.*, 2018, **24**, 209.

21 R. Burgert, H. Schnöckel, A. Grubisic, X. Li, K. H. Bowen, G. F. Ganteför, B. Kiran and P. Jena, *Science*, 2008, **319**, 438–442.

22 M. Neumaier, M. Olzmann, B. Kiran, K. H. Bowen, B. E. S. T. Stokes, A. Buonaugurio, R. Burgert and H. Schnöckel, *J. Am. Chem. Soc.*, 2014, **136**, 3607–3616.

23 T. Iwasa, T. Sato, M. Takagi, M. Gao, A. Lyalin, M. Kobayashi, K.-I. Shimizu, S. Maeda and T. Taketsugu, *J. Phys. Chem. A*, 2019, **123**, 210–217.

24 P. Sazama, L. Capek, H. Drobna, Z. Sobalik, J. Dedecek, K. Arve and B. Wichterlova, *J. Catal.*, 2005, **232**, 302.

25 J. P. Breen and R. Burch, *Top. Catal.*, 2006, **39**, 53–58.

26 D. E. Doronkin, S. Fogel, S. Tamm, L. Olsson, T. S. Khan, T. Bligaard, P. Gabrielsson and S. Dahl, *Appl. Catal., B*, 2012, **113–114**, 228–236.

27 B. W. J. Chen, D. Kirvassilis, Y. Bai and M. Mavrikakis, *J. Phys. Chem. C*, 2019, **123**, 7551–7566.

28 P. Strak, K. Sakowski, P. Kempisty, I. Grzegory and S. Krukowski, *J. Phys. Chem. C*, 2019, **123**, 10893–10906.

29 J. M. Soler, E. Artacho, J. D. Gale, A. García, J. Junquera, P. Ordejón and D. Sánchez-Portal, *J. Phys.: Condens. Matter*, 2002, **14**, 2745.

30 J. Klimes, D. R. Bowler and A. Michaelides, *J. Phys.: Condens. Matter*, 2009, **22**, 02201.

31 N. Troullier and J. L. Martíns, *Phys. Rev. B: Condens. Matter Mater. Phys.*, 1991, **43**, 1993.

32 L. Kleinman and D. M. Bylander, *Phys. Rev. Lett.*, 1982, **48**, 1425.

33 E. M. Fernández and L. C. Balbás, *Phys. Chem. Chem. Phys.*, 2011, **13**, 20863–20870.

34 V. Bonačić-Koutecký, J. Pittner, M. Boiron and P. Fantucci, *J. Chem. Phys.*, 1999, **110**, 3876.

35 P. Weiss, T. Bierweiler, S. Gilb and M. Kappes, *Chem. Phys. Lett.*, 2002, **355**, 355.

36 R. Fournier, *J. Chem. Phys.*, 2001, **115**, 2165.

37 E. M. Fernández, J. M. Soler, I. L. Garzón and L. C. Balbás, *Phys. Rev. B: Condens. Matter Mater. Phys.*, 2004, **70**, 165403.

38 E. M. Fernández, J. M. Soler, I. L. Garzón and L. C. Balbás, *Int. J. Quantum Chem.*, 2005, **101**, 740–745.

39 A. Aguado, A. Vega and L. C. Balbás, *Phys. Rev. B: Condens. Matter Mater. Phys.*, 2011, **84**, 165450.

40 W. Huang and L. S. Wang, *Phys. Rev. Lett.*, 2009, **102**, 153401.

41 J. Claudot, W. J. Kim, A. Dixit, H. Kim, T. Gould, D. Rocca and S. Lebègue, *J. Chem. Phys.*, 2018, **148**, 064112.

42 W. A. de Heer, *Rev. Mod. Phys.*, 1993, **65**, 611.

43 A. C. Reber, G. U. Gamboa and S. N. Khanna, *J. Phys.: Conf. Ser.*, 2013, **438**, 012002.

44 M. Yang, H. Wu, B. Huang and Z. Luo, *J. Phys. Chem. A*, 2019, **123**, 6921–6926.

45 I. Vasiliev, S. Ogut and J. R. Chelikowsky, *Phys. Rev. Lett.*, 1997, **78**, 4805.

46 M. Yang, K. A. Jackson and J. Jellinek, *J. Chem. Phys.*, 2006, **125**, 144308.

47 K. R. S. Chandrakumar, T. K. Ghanty and S. K. Ghosh, *J. Phys. Chem. A*, 2004, **108**, 6661.

48 T. Lünskens, P. Heister, M. Thämer, C. A. Walenta, A. Kartouzian and U. Heiz, *Phys. Chem. Chem. Phys.*, 2015, **17**, 1751.

49 H. Handschuh, C.-Y. Cha, P. S. Bechthold, G. F. Ganteför and W. Eberhardt, *J. Chem. Phys.*, 1995, **102**, 6406.

50 R. F. W. Bader, *Atoms in Molecules: A Quantum Theory*, Clarendon, Oxford, New York, 1990.

51 Y. Zhao, J.-T. Cui, M. Wang, D. Yubero-Valdivielso, A. Fielicke, L.-R. Hu, X. Cheng, Q.-Y. Liu, Z.-Y. Li, S.-G. He and J.-B. Ma, *J. Am. Chem. Soc.*, 2019, **141**, 12592–12600.

52 J. H. Parks, L. Z. J. Ho and S. J. Riley, *J. Chem. Phys.*, 1994, **100**, 7206–7222.

53 E. F. Rexer, J. Jellinek, E. B. Krisinel and E. K. Parks, *J. Chem. Phys.*, 2002, **117**, 82–94.

54 P. K. Chattaraj, *Chemical Reactivity Theory: A Density Functional View*, CRC Press, Taylor and Francis Group, Boca Raton, FL, 2009.

55 T. M. Bernhardt, *Int. J. Mass Spectrom.*, 2005, **243**, 1–29.

56 E. M. Fernández, P. Ordejón and L. C. Balbás, *Chem. Phys. Lett.*, 2005, **408**, 252–257.

57 M. B. Torres, E. M. Fernández and L. C. Balbás, *J. Phys. Chem. A*, 2008, **112**, 6678.

58 M. Schmidt, A. Masson and C. Bréchignac, *J. Chem. Phys.*, 2005, **122**, 134712.

59 M. V. den Bossche and H. Grönbeck, *J. Phys. Chem. C*, 2017, **121**, 8390–8398.

60 S. Abujarada, *et al.*, *Phys. Chem. Chem. Phys.*, 2019, **21**, 10939.

61 N. Takagi, K. Ishimura, R. Fukuda, M. Ehara and S. Sakaki, *J. Phys. Chem. A*, 2019, **123**, 7021–7033.

62 T. Ghanty and S. K. Ghosh, *J. Phys. Chem.*, 1996, **100**, 12295.

63 T. Kamachi, T. Tatsumi, T. Toyao, Y. Hinuma, Z. Maeno, S. Takakusagi, S. Furukawa, I. Takigawa and K. Shimizu, *J. Phys. Chem. C*, 2019, **123**, 20988–20997.